WOOD MATERIAL SCIENCE & ENGINEERING, 2018
https://doi.org/10.1080/17480272.2018.1458049

Taylor & Francis
Taylor & Francis Group

Fungal–copper interactions in wood examined with large field of view synchrotron-based X-ray fluorescence microscopy

Samuel L. Zelinka[a], Joseph E. Jakes[a], Juliet Tang[b], Katie Ohno[a], Amy Bishell[a], Lydia Finney[c], Evan R. Maxey[c], Stefan Vogt[c] and Grant T. Kirker[a]

[a]USDA-FS Forest Products Laboratory, Madison, WI, USA; [b]USDA-FS Forest Products Laboratory, Starkville, MS, USA; [c]Argonne National Laboratory, Advanced Photon Source, Lemont, IL, USA

ABSTRACT

The goal of this study was to demonstrate how synchrotron-based X-ray fluorescence microscopy (XFM) can be used to better understand the mechanisms of copper tolerance in wood decay fungi. Copper is a major component in commercial wood preservatives as it is toxic to many wood decay fungi. However, certain fungi are copper tolerant and can attack preservative-treated wood, resulting in structural damage to treated wood members. Here we used large-field XFM to visualize six different elements (K, Ca, Mn, Fe, Cu, and Zn) in the mycelia and wood inoculated with four different species of brown rot wood decay fungi. Wood blocks were partially dipped into a solution of copper sulfate, exposed to fungi in malt extract agar petri dish assays for nine weeks, and then imaged and compared to blocks that were partially dipped in water. The blocks were imaged immediately adjacent to an end-matched control that was placed in malt extract agar petri dish assays for 9 weeks, but not exposed to the fungi so that the differences in the elemental distributions could be directly compared. The colonized wood and mycelia were rich in K, Ca, Mn, and Fe; however, the elements and the spatial distribution in the mycelia and wood differed across fungal species. The most interesting results were the maps showing the copper distribution. While three of the four fungi grew on the copper-rich region of the wood, only one species, *Fibroporia radiculosa*, dramatically reduced the copper concentration in the region of fungal growth.

ARTICLE HISTORY
Received 20 October 2017
Revised 1 March 2018
Accepted 23 March 2018

KEYWORDS
Wood decay; brown rot fungi; *Fibroporia radiculosa*; ion translocation

1. Introduction

Wood used in outdoor applications is susceptible to decay. Waterborne preservative treatments specified for wood used in outdoor applications hinder fungi through repellent, biostatic, or biocidal actions; almost all commercially available waterborne preservatives currently on the market rely on the toxicity of copper to decay fungi (Lebow 2010). In the United States, the most common waterborne wood preservative was chromated copper arsenate (CCA), which was composed of the salts of hexavalent chromium oxide, cupric oxide, and arsenic pentoxide (Lebow 2004). This three-part preservative was shown to be highly effective at preventing wood decay and insect attack (Lebow *et al.* 2013). However, voluntary regulation changes requested by CCA registrants resulted in CCA being withdrawn from use in residential construction in 2004 (Burkholder 2004, Lebow 2004). Following this regulation change, many different wood preservatives have been introduced to the marketplace (Lebow 2004, 2010). In general, these wood preservatives have an increased reliance on copper (they contain much higher proportions of copper than CCA), and incorporate an organic co-biocide – typically quaternary ammonia compounds or azoles to control copper-tolerant molds/mildews (Zelinka 2014). Similarly, in the European Union, increased environmental concerns and the high cost of pesticide registration have drastically reduced the number of registered biocides so that copper and creosote are the only two remaining active chemical ingredients registered for use in wood impregnation for use in ground contact or marine exposure (Anon. 2017, Jones and Brishke 2017).

While copper is fungicidal to many wood decay fungi, certain fungi are copper tolerant. Copper tolerant fungi have the ability to reduce bioavailability and translocate copper (Tang *et al.* 2013) from wood treated with copper-based preservatives. Copper tolerant brown rot fungi have been studied for over 30 years (Murphy and Levy 1983, Hastrup *et al.* 2005). Copper tolerant fungi secrete high amounts of oxalate in wood treated with copper (Clausen and Green 2003, Green and Clausen 2003). The exact role of oxalate in copper tolerant fungi is not fully understood, Humar *et al.* (2002) evaluated tolerance of select fungi to copper octanoate with ethanolamine or copper (II) sulfate treated Norway spruce followed by analysis of copper forms using electron paramagnetic resonance (EPR) and found that copper (II) sulfate was transformed in the wood by most of the test fungi to insoluble copper oxalate. The presence of ethanolamine, however, hindered the production of copper oxalate and prevented decay. The results of these tests indicate that copper (II) sulfate can be transformed into insoluble and non-biocidal forms that allow even non-copper tolerant fungi to cause mass loss. Subsequent analysis

CONTACT Grant T. Kirker gkirker@fs.fed.us

of the underlying media showed that even though copper was transformed in the wood, very little was lost via leaching into the media underneath. Humar *et al*. (2005) examined EPR spectra of copper/chromium/boron (CCB) treated wood exposed to several copper tolerant fungi and compared them to CCB treated wood exposed to organic and inorganic acids. Both treatments significantly impacted the decay resistance of the CCB treated wood indicating that similar mechanisms are involved in the development of copper tolerance (i.e. acidification of the substrate). EPR spectra were very similar between the fungus exposed and acidified wood and after acidification, normally copper sensitive wood decay fungi were able decay the CCB treated wood.

In *Fibroporia radiculosa*, previous studies have found that growth on copper preservative-treated wood increased expression of genes not only involved in oxalate metabolism, but also genes in two other metabolic cycles that were linked to oxalate production (Tang *et al*. 2013, 2016). These data provide that the sequestration of soluble extracellular copper into insoluble copper-oxalate crystals (Schilling and Inda 2011) is at least partly involved in the detoxification mechanism the underlies copper tolerance. Studies investigating the intracellular removal of copper comes from gene expression work by Tang *et al*. and Ohno *et al*. who examined the copper-tolerant brown rot fungus *F. radiculosa* (Tang *et al*. 2013, 2016, Ohno *et al*. 2016), these being involved in the translocation the oxalate-sequestered copper away from the fungus; however, these measurements were not spatially resolved, and to date, have yet to directly visualize fungus–copper interactions.

Recently, Kirker *et al*. (2017) showed how synchrotron-based X-ray fluorescence microscopy (XFM) can be used as a tool for understanding ions and wood decay fungi. Kirker *et al*. examined *Serpula lacrymans* grown on untreated wood using XFM. The XFM maps were able to show ion translocation from the soil into the wood at both the millimeter and micron length scales in both the fungal hyphae and the wood cell walls. Because XFM allows the elemental composition to be determined down to trace compositions at high spatial resolution, it is ideally suited for studying how copper tolerant fungi interact with copper in treated wood.

Here we show how synchrotron-based XFM can be used as a tool to examine mechanisms of copper tolerance in wood decay fungi. In these experiments, fungi were grown on wood with a diffused copper gradient and the elemental profiles were mapped and compared to matched controls with no fungi. Comparisons were also made to wood blocks treated with water. Comparisons between these experiments can help us to better understand copper tolerance and the protective mechanisms that copper tolerant fungi use to survive and grow on wood treated with copper-based preservatives.

2. Materials and methods

In brief, the experiment consisted of four steps: wood samples were cut, dipped in a treatment solution, exposed to a fungus (or control) and then imaged with X-ray fluorescence microscopy. All chemicals were purchased from Sigma-Aldrich (St. Louis, MO) and are laboratory grade unless otherwise mentioned.

Southern pine (*Pinus spp*.) sapwood (33 mm × 26 mm × 5 mm, 4 replicates per fungus) was cut into two equal pieces across the grain. Prior to dip treatment, these test blocks were equilibrated in a 70°C: 30% RH environmental growth chamber to 12% MC. The end-matched pairs were then held together and partially dipped into a solution made from 2.36 g of copper sulfate pentahydrate in 100 mL of water to a depth of 10 mm for 30 s. The resulting total copper retention was calculated as 86 g of copper per m^3 of wood. This dip pattern produced a copper concentration gradient, and allowed observation of how fungi interacted as they approached the copper-rich region. In addition to the samples dipped in the copper solution, control measurements were taken on wood samples dipped in deionized water.

After the treatment, samples were allowed to dry for 10 min. After the drying period, one of the end-matched samples was placed on top of a plastic grid ("gutter guard") in a sterile, uninoculated petri dish containing 2% malt extract agar. The second end-matched sample was then placed into a petri dish with 2 plugs (5 mm plug diameter) of fungus added, one on the dipped edge and one on the opposite edge. Four brown rot fungi were examined: *Gloeophyllum trabeum* (Pers.:Fries) Murrill (MAD-617), *Postia placenta* (Fr.) Lars. & Lombard (MAD-698), *F. radiculosa* (TFFH-294), and *Fomitopsis palustris* (Berk. & Curt.) Murr. (TYP-6137). *G. trabeum was* chosen as a non-copper tolerant control (Green and Clausen 2003, Guillén and Machuca 2008). *F. radiculosa and F. palustris* were chosen as these fungi are known to be highly copper tolerant (Green and Clausen 2003). *P. placenta* was chosen because it is mildly copper tolerant (Green and Clausen 2003). Petri dishes were then maintained at 30°C and 70% relative humidity for 9 weeks, after which the specimens were removed, oven dried overnight at 105°C and weight loss was measured by comparing pre and post-test oven dry weights. Nine weeks was selected based on observations from previous studies using XFM to visualize metal ions in fungus colonized wood and scaled accordingly based on the sample dimensions and fungal exposure conditions.

After the test was over, the end-matched samples were mounted next to each other on a sample rack to be imaged at the beamline (Figure 1). This experimental configuration allowed us to directly compare the elemental concentration profile for wood that had been in contact with each fungus with an end-matched control exposed to similar conditions, but without each fungus.

The XFM was performed at the 8-BM beamline at the Advanced Photon Source (APS) at Argonne National Laboratory (Argonne, IL, USA). The beamline provides large field-of-view fluorescence maps. The incident X-ray beam energy was 10.1 keV, and the spot size was approximately 30 µm wide by 20 µm high. The sample was raster-scanned using 40 µm steps with 100 ms dwell times at each step to build elemental maps. Because of the penetrating nature of hard X-rays, which can reach a few hundred microns into the surface depending on sample density, the images represented a 2D area projection of a 3D volumetric measurement.

In most measurements, the fungal growth was left intact while the samples were imaged (e.g. Figure 1). Preliminary measurements, however, were performed to determine

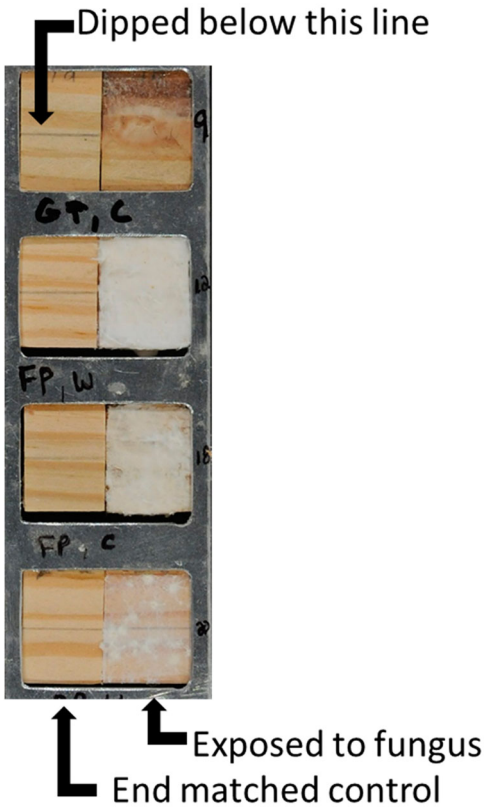

Figure 1. Samples mounted in the sample rack for XFM data collection. End-matched wood specimens were imaged together to directly compare the effect of the fungus. The pencil line on the sample represents the depth to which the wood was dipped in a copper sulfate or water solution.

whether the X-rays could penetrate the fungus. The mycelium was partially scraped from the wood surface and an image was taken that included both the scraped and unscraped regions. These measurements were useful for understanding how much of the X-ray signal was absorbed by the fungus and how the elemental signals were partitioned between the wood and the fungi.

XFM data were visualized with the MAPS software package, where the full spectra were fit to Gaussian peaks, background iteratively calculated and subtracted (Vogt 2003). The results were compared to standard reference materials (RF8-200-S2453, AXO GmbH, Dresden). For the data presented herein, the elements analyzed were potassium (K), calcium (Ca), manganese (Mn), iron (Fe), copper (Cu), and zinc (Zn), and all elemental maps for a given element were scaled to the same color intensity so that direct comparisons could be made between the figures. These were deemed to be the main elements of interest based on their roles in fungal physiological processes and actions of wood preservatives. Cu was the main element of interest as the goal is to track the movement of copper as copper-tolerant fungi colonize cu-treated wood. Zn is selected as a marker for wood cell wall based on prior studies of wood cell walls using XFM (Zelinka *et al*. 2015). Ca is strongly correlated with the presence of fungal hypha, while K is a highly mobile cation in fungal cells and based on prior studies is positively correlated with hyphae which does not co-locate with Fe, Mn or Zn (Kirker *et al*. 2017).

3. Results

Figure 2 presents the weight loss data after the wood blocks had been exposed to each fungus for 9 weeks on 2% malt extract agar. Because of the high variance and the small number of replicates ($n = 4$ for each species, exposure, and dip combination), there was no statistical difference between the blocks dipped in copper and those dipped in water within or across species. The highest weight losses were seen in *F. palustris* and *P. placenta*. These high weight losses correlated well with a high coverage of mycelium on the top of the wood blocks that were later imaged. Moderate weight losses and dense mycelium coverage were observed for *F. radiculosa*. The blocks that were dipped in copper and exposed to *G. trabeum* had the lowest mean weight loss, which was consistent with the a priori hypothesis of using this fungus as a non-tolerant control. In these blocks, mycelium was only visible on the top portion of the block that was not dipped in copper (see the top frame of Figure 1).

Figure 3 shows how the fungal mycelium affected the XFM maps and absorption of the X-ray beam and fluoresced photons. In this preliminary experiment on a fully copper-treated block exposed to *P. placenta*, approximately half the surface was scraped to remove the surface mycelium prior to imaging (Figure 3(a)). The elemental profile of the mycelium contained high amounts of K and Ca, which can be seen in Figure 3(b,c), respectively, and was reduced upon scraping. Both the K and Ca maps have vertical features in the maps that correspond to the boundary between the scraped and non-scraped regions. Finally, the observed copper distribution in the wood is shown in Figure 3(d). No differences were seen in the copper concentration between the scraped and unscraped regions, which suggests that the fungal mycelium was not absorbing enough X-rays or fluoresced photons to affect the measurement. The XFM maps therefore depict a 2D representation of ions from a combination of the fungal mycelium on the wood surface and the elements near the top surface of the wood block in both the wood cell walls and mycelium occupying the cell lumina.

The remainder of the images presents data with an end-matched control specimen to directly compare the effect of each fungus. Example images are presented and discussed.

Figure 4 contains photographs and elemental maps for wood exposed to *G. trabeum*. The mycelial coverage in the water-dipped specimen (Figure 4(a)) was sparse and extended over the entire surface of the block. This was in sharp contrast with the copper-dipped block (Figure 4(h)), where there was dense coverage of mycelia in the upper half of the block, but no growth in the bottom half of the block except closest to the dip line. For the blocks dipped in water, the overall concentrations of K, Ca, and Mn were higher in the block exposed to the fungus than the control (Figure 4(b–d)). The distribution of K, Ca, and Mn for the water-dipped blocks exposed to fungus varied. K was uniform (Figure 4(b)), while Ca and Mn were both higher in the top half of the block (Figure 4(c,d)). Similar trends were observed for these three elements in the copper-dipped block (Figure 4(i–k)), except that the higher concentrations in the exposed block were always restricted to half above the copper dip

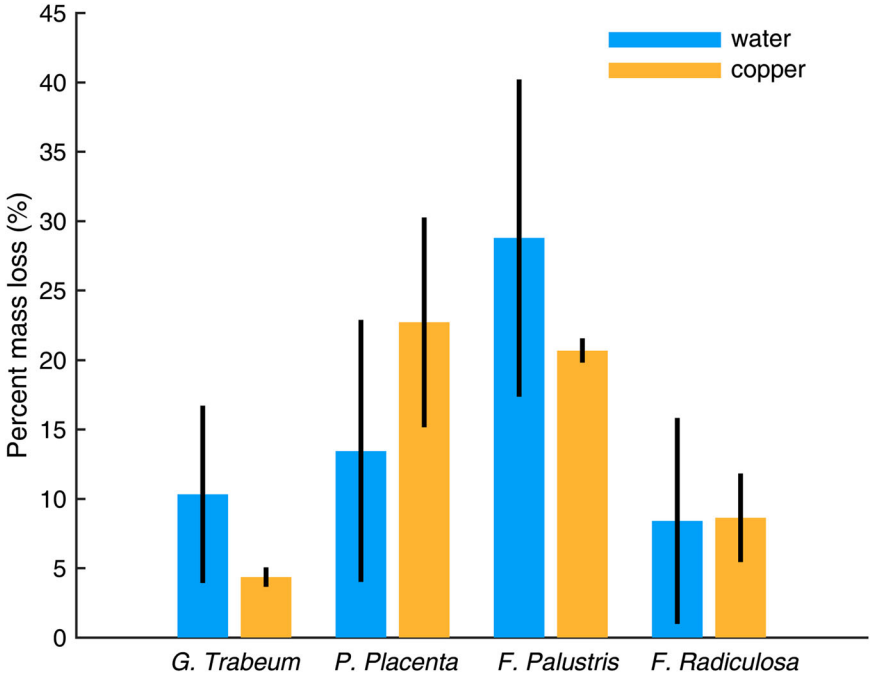

Figure 2. Mass loss caused by decay measured on copper and water-dipped southern pine test wafers exposed for 9 weeks to four brown rot fungi with varying levels of copper tolerance.

Note: The error bar represents the standard error ($n = 4$).

line, even for K. No difference in Zn concentration was discernible in either treatment (Figure 4(g,n)).

In comparing the amount of Fe in the water and copper-dipped blocks (Figure 4(e) vs. Figure 4(l)), it appeared that there were higher amounts of Fe in the block that was dipped in copper. Furthermore, the amount of Fe was higher not just in the block exposed to the fungus, but also in the end-matched control. We believe that this was not a different response from the fungus, but rather originated from trace amounts of Fe in the copper sulfate solution (note that the scale of the Fe map is 80 times more sensitive than that of the Cu map).

Figure 4(f,m) show the elemental maps of Cu. Although there was little to no Cu detected throughout the water-dipped wood (Figure 4(f)), the Cu in the copper-dipped wood exhibited different patterns depending upon whether it was exposed or not exposed to the fungus (Figure 4(m)). The Cu concentration appeared to be lower in the block that was exposed to fungus when compared to its end-matched control. Notably, it appeared that the Cu had diffused past the original dip-line during the experiment (top, right of Figure 4(m)). However, in the sample exposed to the fungus, this region seemed to have a much lower Cu concentration. Although the fungus did not progress much past the intended Cu dip line, the Cu concentration appeared to be slightly lower than the control up to 3 mm above from the dip line.

Figure 5 presents photographs and XFM images of wood exposed to *P. placenta*. The mycelial coverage in Figure 5(a, h) of wood dipped in water and copper, respectively, showed a much thicker coverage than was observed for *G. trabeum*. The fungus appeared to cause cracks in the wood that were not observed in the end-matched control; cracks were visible 8 mm from the bottom surface on the water-dipped block and 4 mm from the top surface on the copper-dipped block. These cracks were likely an artifact from exposure to the decay fungi followed by oven drying. The block that was dipped in water and exposed

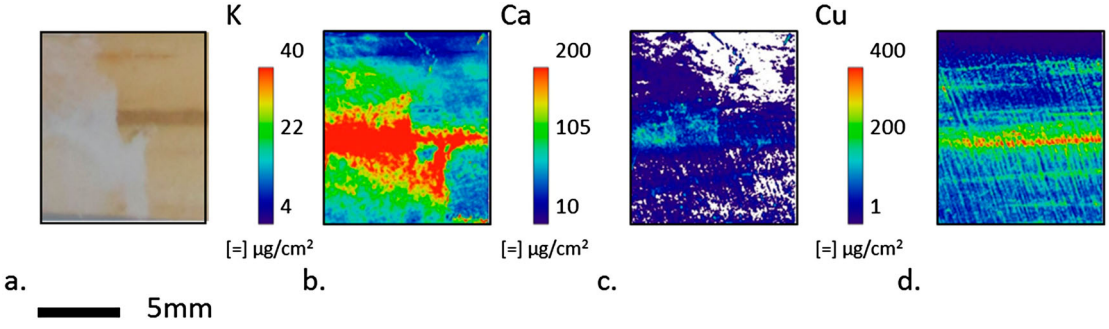

Figure 3. Images of a fully dipped copper-treated block exposed to the fungus *P. placenta*. A photograph showing scraped and unscraped mycelial regions (a). XFM images of K (b), Ca (c), and Cu (d) for the same area shown in (a). The Cu signal (d) is unchanged between the scraped and unscraped regions.

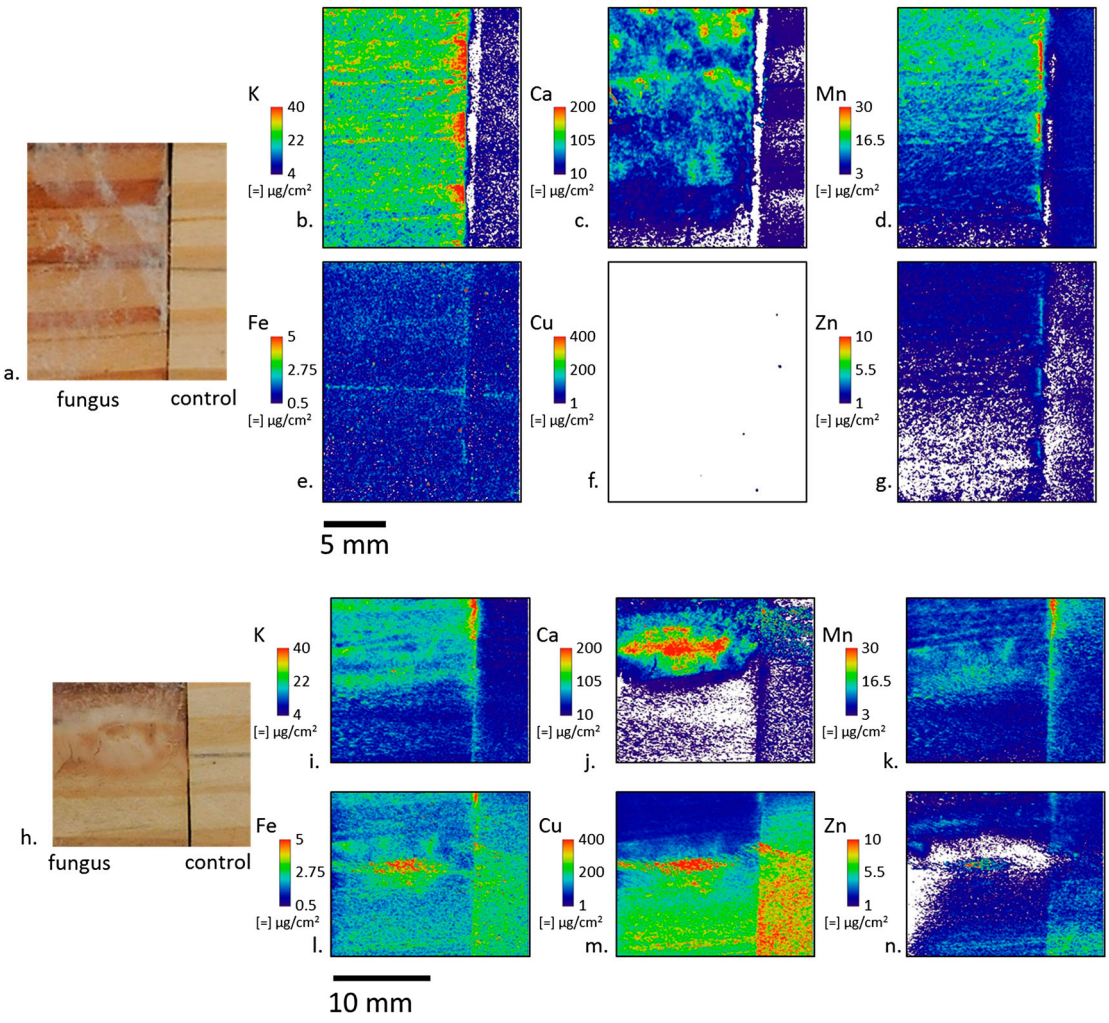

Figure 4. Images (a,h) and associated XFM maps of samples exposed to *G. trabeum*. Subfigures a–g and h–n were dipped in water and copper, respectively. The left and right side of each image, labeled "fungus" and "control", were exposed and not exposed to fungus, respectively. The lower half of the sample (below the pencil line) was dipped in the solution.

to the fungus had noticeably higher amounts of K (Figure 5(b)) and Mn (Figure 5(d)) than the end-matched control. For Mn, in addition to a broadly distributed higher concentration, there also appeared to be a band of hotspots (<250 µm in diameter) with high Mn concentration about 5 mm below the top of the image (Figure 5(d)). This band of hot spots was also noticeable in the Zn map (Figure 5(g)). It was unclear what these hot spots corresponded with physically. For the water-dipped blocks, the maps for Fe and Cu (Figure 5(e,f)) show low concentrations of both elements and little if any noticeable changes between the exposed and control blocks.

Both water and copper-dipped samples had higher amounts of K (Figure 5(b,i)) in the exposed block relative to the controls. However, the K map from the copper-dipped block (Figure 5(i)) exhibited a different spatial distribution than in the one dipped in water (Figure 5(b)). There was also a region of high Ca concentration in the portion of the block dipped in copper (Figure 5(j)) and the highest region of Ca collocated with the highest region of Cu (Figure 5(m)). This was interesting as the amount of Ca in the exposed water-dipped block was similar to the control (Figure 5(c)).

The Mn map of the copper-dipped blocks (Figure 5(k)) was difficult to interpret. The control side of the block is very small in this image. The control block had a much higher concentration of Mn than the water-dipped control block (Figure 5(d)). In addition, for large maps (14 mm × 17 mm, not shown) of control, undipped samples, the Mn concentration ranged from 5 to 7 µg cm^2, roughly half of what was found in this small control sliver of the copper-dipped block. Therefore, it is unclear if the entire control had a high concentration or if the high concentration seen in the map was an experimental artifact. The concentration of Mn in the copper-dipped block exposed to fungus was similar to both the concentration of the water-dipped block (Figure 5(d)) exposed to fungus and its edge matched copper-dipped but unexposed counterpart. Because of this, it was impossible to determine if this increased Mn concentration (relative to other control samples) was caused by a higher amount of Mn in this particular sample or instead caused by the fungus.

The overall Cu concentration appeared similar between the block exposed to the fungus and the end-matched control (Figure 5(m)). It appeared that the Cu front diffused further in the control sample and that there may have been

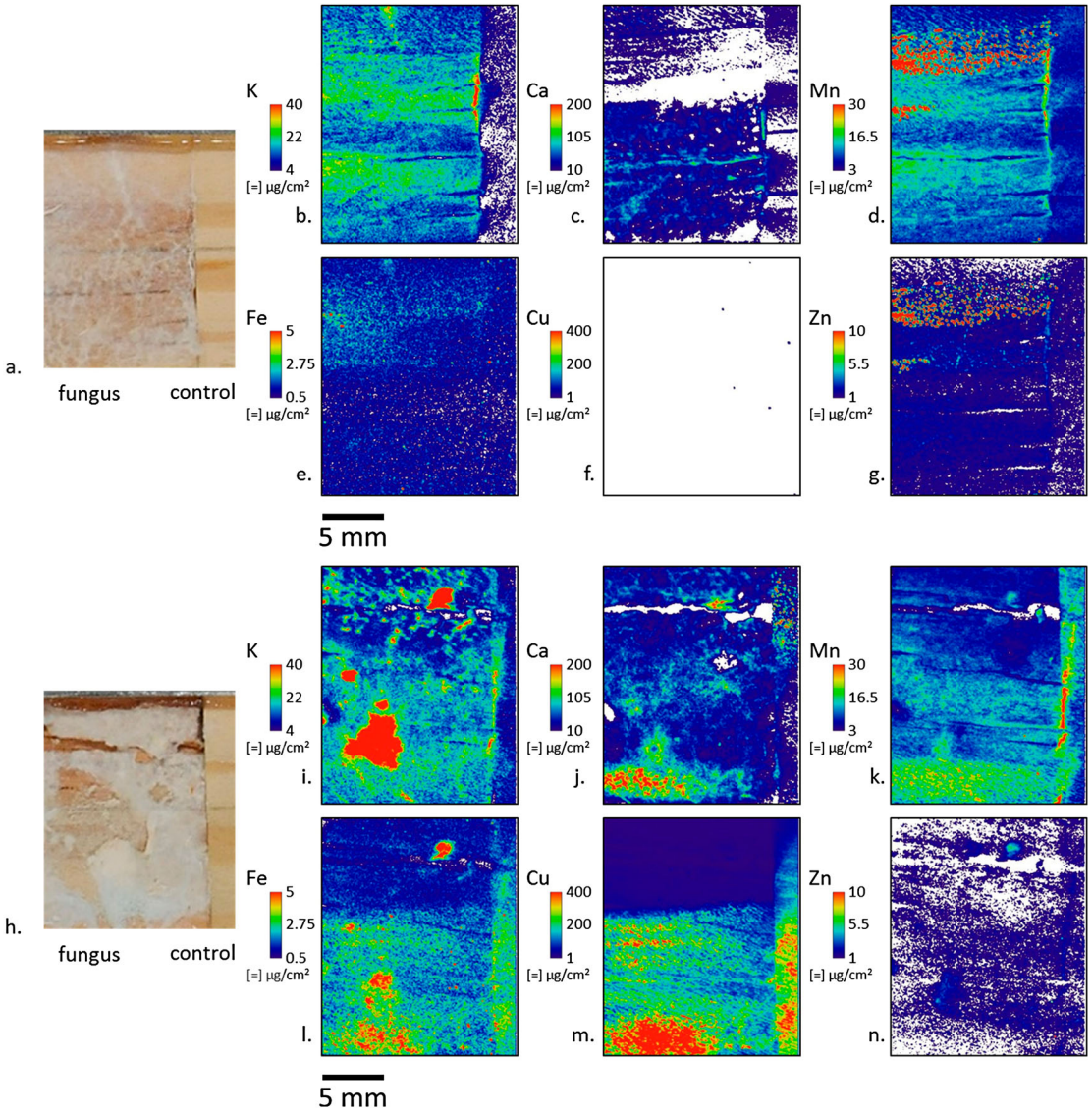

Figure 5. Images (a,h) and associated XFM maps of samples exposed to *P. placenta*. Subfigures a–g and h–n were dipped in water and copper, respectively. The left and right side of each image, labeled "fungus" and "control", were exposed and not exposed to fungus, respectively. The lower half of the sample (below the pencil line) was dipped in the solution.

a slight reduction in the Cu concentration in the block exposed to the fungus. A similar pattern could be seen in the Fe map, (Figure 5(l)) noting that the Fe in the control block was introduced from impurities in the copper sulfate.

Figure 6 presents images and XFM maps of wood exposed to *F. palustris*. The images (Figure 6(a,h), wood dipped in water and copper, respectively) showed that there was a thick coverage of mycelium on the surface of both blocks. In the water-dipped blocks, there was a higher amount of Ca (Figure 6(c)) and Mn (Figure 6(d)) in the block that was exposed to the fungus than the end-matched control. These elements were not uniformly distributed, but instead existed in oval-shaped nodules (~1 mm) of high concentration. Interestingly, the regions of high Ca concentration are not correlated with the regions of high Mn concentration. Unlike the other fungi examined, there was not a dramatic difference in the K signal between the block exposed to fungus and the end-matched control for both the water and copper-dipped samples (Figure 6(b,i)). Similar to K, little changes were observed between the exposed and unexposed samples in the Fe, Cu, and Zn maps for the water-dipped samples (Figure 6(e–g)).

For the copper-dipped block, little difference was observed between the exposed and unexposed samples in the concentrations of K, Fe, and Zn (Figure 6(i,l,n)). The Ca profile in the copper-dipped block was similar to that in the untreated block (Figure 6(j)); both exhibit nodules, although the water-dipped block had more nodules than the copper-dipped block. Similar to *P. placenta*, the Mn map of the copper-dipped block exposed to *F. palustris* (Figure 6(k)) is difficult to draw definitive conclusions from, with higher than expected concentrations of Mn in both the control and exposed samples.

The Cu concentration map (Figure 6(m)) exhibited similar trends to that observed in *G. trabeum* and *P. placenta*, though a higher concentration overall. The Cu front diffused

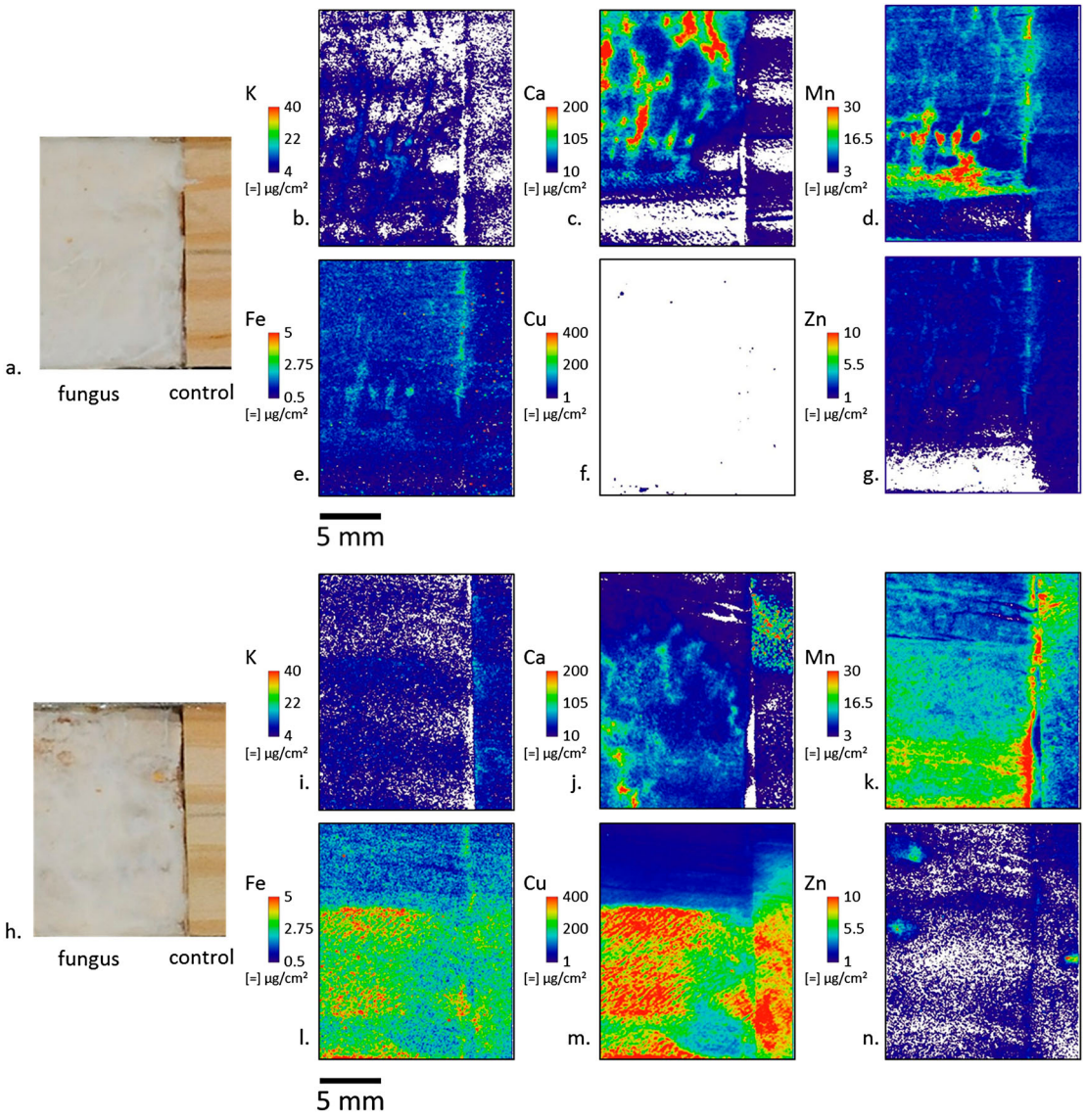

Figure 6. Images (a,h) and associated XFM maps of samples exposed to *F. palustris*. Subfigures a–g and h–n were dipped in water and copper, respectively. The left and right side of each image, labeled "fungus" and "control", were exposed and not exposed to fungus, respectively. The lower half of the sample (below the pencil line) was dipped in the solution.

further in the end-matched control than in the block that was exposed to the fungus. Furthermore, it appeared that the overall Cu concentrations were similar or slightly lower in the exposed block relative to the control.

Figure 7 presents images and XFM maps of samples exposed to *F. radiculosa* along with end-matched controls. The mycelial coverage extends the entire length of the block for both the water and copper-dipped samples (Figure 7(a,h)), although the coverage does not appear to be as thick as for *P. placenta* and *F. palustris*. Although there were no cracks caused by the fungus growing on the water-dipped block (Figure 7(a)), the block dipped in copper and exposed to fungus had several cracks caused by the fungus (Figure 7(h)); the dark brown region on the bottom of Figure 7(h) was from epoxy that was used to hold the sample together for XRF imaging. As stated previously, it is acknowledged that these cracks are likely artifacts from the drying process but these are also indicative of brown rot decay of wood and the fact that the Cu treated blocks exhibited higher instances of cracking are unclear.

For the sample dipped in water and exposed to *F. radiculosa*, there were higher amounts of K (Figure 7(b)) and Fe (Figure 7(e)) than in the controls. Both the K and Fe concentrations were evenly distributed throughout the sample exposed to fungus and higher than any other species of water-dipped fungal exposed wood. No differences in Ca, Mn, Cu, or Zn could be observed between the exposed and control samples (Figure 7(c,d,f,g)).

The elemental maps from the blocks that were dipped in copper and then exposed to *F. radiculosa* (Figure 7(i–n)) exhibited key differences from the elemental maps of the water-dipped blocks. While the K was higher in the exposed block, there was a much higher concentration of K below the copper dip line than above it. Likewise, there was a much higher amount of Mn below the dip line in the exposed block (Figure 7(k)), although it is again difficult to interpret

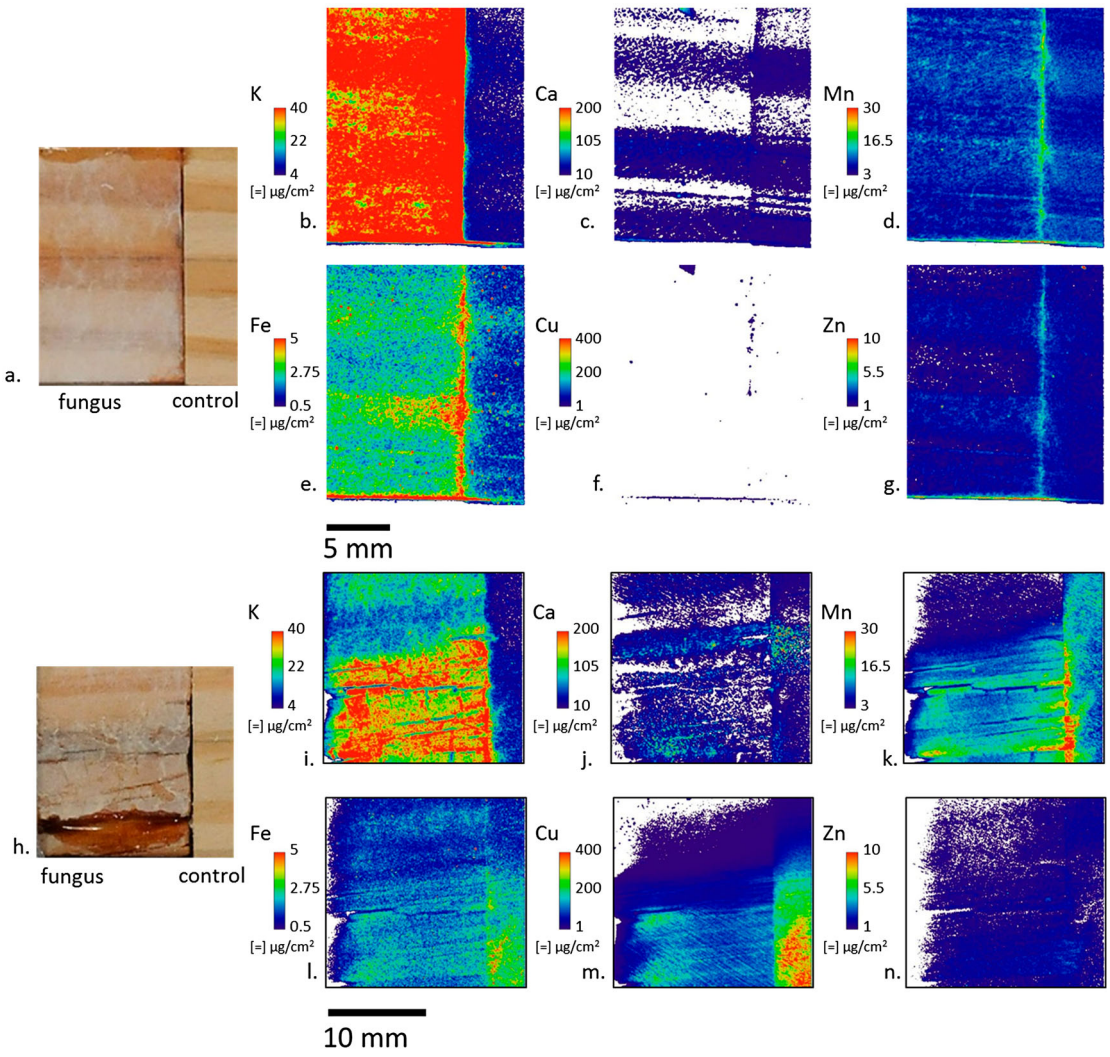

Figure 7. Images (a,h) and associated XFM maps of samples exposed to *F. radiculosa*. Subfigures a–g and h–n were dipped in water and copper, respectively. The left and right side of each image, labeled "fungus" and "control", were exposed and not exposed to fungus, respectively. The lower half of the sample (below the pencil line) was dipped in the solution.

since the unexposed control also had a higher amount of Mn. The Zn concentration appeared to be lower in the fungal exposed block (Figure 7(n)). No changes were observable in the Ca maps between the exposed and control samples (Figure 7(j)).

For the copper-dipped blocks, the most interesting XFM maps were the Cu (Figure 7(m)) and Fe (Figure 7(l)) maps. The block that was exposed to *F. radiculosa* had less Cu than the end-matched control. It appeared that the fungus removed Cu from the surface of the block. Furthermore, the concentration of Fe was less than the end-matched control. This was an especially interesting result since, for the water-dipped block, it appeared that the fungus increased the Fe concentration (Figure 7(e)), whereas in the copper-dipped block the concentration was lower than its end-matched control (Figure 7(l)).

4. Discussion

This work utilized the high elemental sensitivity of XFM to examine how different wood rot fungi interacted with copper-treated wood. Matched samples allowed direct comparisons between the wood that had been exposed to fungus and wood that was exposed to the same environmental conditions without fungal exposure. Additional comparisons were made for each fungus between wood partially treated with a copper solution and wood partially treated with water. Measurements where the mycelium was partially scraped away from the wood surface suggested that the X-rays could easily penetrate the fungus, and the resulting image maps represent the combined elemental concentrations of the fungus and the wood. While these XFM maps represent only one time point along the decay process (9 weeks) and are limited to the four fungi examined as well as their three replicates, the data presented in this work give insight into the mechanisms of copper tolerance, as well as show how synchrotron-based XFM can be used to better understand copper tolerance in brown rot fungi and the mechanism of wood decay in general.

The mycelial coverage was indicative of where the fungus affected the elemental concentrations. However, depending upon the fungal species, the distribution and concentration

Table 1. Summary of elements that increased in the block exposed to fungus relative to the end-matched controls.

	Dip treatment	
	Water	Copper
G. trabeum	K, Ca, Mn	–
P. placenta	K, Mn	K, Ca, Mn[a]
F. palustris	Ca, Mn	Ca, Mn[a]
F. radiculosa	K, Fe	K, Mn[a]

The "Copper" column refers to elements that increased in the copper-rich region, below vs. above the dip line.
[a]The Mn concentration was higher than for untreated wood. However, the end-matched controls also exhibited a higher than normal concentration.

of these elements could not be determined solely from the local abundance of mycelial coverage. Differences in the elemental signatures were observed between fungi. These are highlighted in Table 1, which lists the elements that had a noticeably higher concentration in the blocks exposed to each fungus. Two fungi, *P. placenta* and *F. radiculosa*, exhibited different ion signatures in mycelium when exposed to copper. Previous work, based on bulk measurements of ions in decayed wood using inductively coupled plasma spectrometry have concluded that ion translocation is used by fungi to modify their environment and colonize wood (Jellison *et al*. 1997, Ostrofsky *et al*. 1997, Schilling and Jellison 2007), however, interspecies comparisons of the types and quantities of translocated ions are lacking. The differences in the elemental signatures of the mycelium suggest that these brown rot fungi utilize different ions and have key differences in their metabolic pathways. Furthermore, two of the fungi have different ion signatures in the presence of copper suggesting that the copper influences ion translocation.

Among the four fungi, three different responses to the copper treatment could be observed. *G. trabeum* was unable to grow on the copper-containing wood and its growth stopped at the copper interface in the wood. Both *P. placenta* and *F. palustris* were able to grow on the copper-containing regions in the wood and the copper concentration was slightly lower than the control. Finally, *F. radiculosa* was also able to grow in the copper-containing region, but, in this case, the copper concentration was dramatically lower in the colonized sample. The copper sulfate solution appeared to have trace amounts of Fe, which can be seen in the end-matched controls of all samples dipped in the copper sulfate solution. *G. trabeum*, *P. placenta*, and *F. palustris* did not affect the Fe concentrations. However, the block colonized by *F. radiculosa* contained less Fe than its end-matched control (Figure 7(l)). This is especially interesting given that in the control block (Figure 7(e)) *F. radiculosa* increased the amount of Fe within the block. Apparently, *F. radiculosa* can manipulate Fe concentrations according to the environmental concentrations of copper

The unexposed copper-dipped blocks also appeared to have higher Mn concentrations than the water-dipped samples. However, unlike the Fe profiles, the higher Mn regions did not correspond to the dip pattern. While on average, these blocks all had higher Mn concentrations, the higher amounts of Mn in some cases appeared at the top of the block (Figure 4(k)) far away from the dip line. If the Mn was introduced in the dip treatment, then the Mn must have a much higher diffusion in the wood than Cu or Fe. The inconsistent presence of extra Mn in the unexposed copper-dipped samples makes a complete analysis of the effect of copper on the Mn distribution impossible.

One of the strongest findings was that there were differences in the fungal–copper interactions between the three copper tolerant fungi: *P. placenta*, *F. palustris*, and *F. radiculosa*. All three of these fungi grew over the copper dip line. In *F. radiculosa* wood copper concentrations were greatly lowered by the fungus, whereas in the other copper-tolerant fungi, the fungi were able to grow in areas of high copper concentration. Gene expression work on copper tolerance in *Fibroporia* has highlighted a role for P-type ATPase pumps as a potential copper tolerance mechanism (Tang *et al*. 2013, 2016, Ohno *et al*. 2016). Since cell membranes are inherently leaky, organisms living in environments with high concentrations of heavy metals must have a mechanism for transporting and utilizing these micronutrients in trace amounts within the cell, while simultaneously preventing intracellular concentrations from becoming toxic. The P-type ATPase pumps serve this function. They span the plasma membrane and act as efflux pumps, selectively transporting heavy metals out of the cytoplasm back to the environment. It is conceivable then that differences in efflux rates and metal specificity of the P-type ATPase pumps could account for the range of copper tolerances observed (Argüello *et al*. 2007).

Several mechanisms of copper tolerance are in play and vary in their relative contribution depending upon the species. *F. radiculosa* is a species that is capable of forming mycelial cords (Bernicchia *et al*. 2012), which can function in water and ion translocation (Duddridge *et al*. 1980). Translocation may explain why the concentration of copper in the copper-treated wood was lower after exposure to *F. radiculosa*. In this case, a strategy that combines copper pumps with copper translocation via mycelial cords may act together to confer copper tolerance.

High levels of oxalate have been correlated with copper-tolerant fungi growing in wood treated with copper-based preservatives (Clausen and Green 2003) and up-regulation of oxalate-producing genes has been observed in *F. radiculosa* (Clausen and Green 2003, Tang *et al*. 2013). While the data presented here did not specifically map out the oxalate concentrations in the wood, it has been shown by scanning electron microscopy energy-dispersive X-ray spectroscopy that brown rot fungi use oxalate to sequester copper in a copper-oxalate crystal (Clausen *et al*. 2000, Tang *et al*. 2013). The resolution of the elemental maps (40 µm) was too coarse to resolve potential copper-oxalate crystals within the wood; however, a different beamline at APS is able to take similar XFM maps with a resolution of approximately 500 nm. Kirker *et al*. (2017) used this beamline to map and quantify Ca, Mn, and other ions present in calcium oxalate crystals produced by *Serpula lacrymans* in untreated wood. It may be possible in future work to examine these specimens at the high-resolution beamline to see whether copper-oxalate crystals can be found in any of the copper tolerant fungi. If differences in the number, morphology, and composition, of crystals are found between species, it may suggest that some fungi detoxify copper by elemental

transformation rather than translocation away from the hyphae. The results of these experiments do not provide enough spatially resolved data to elucidate the relationships between Cu oxalate formation and copper tolerance and more controlled experiments using a less expensive method, such as SEM-EDX could provide useful information to substantiate these relationships.

The observed differences in elemental maps (particularly for K and Cu) between *F. radiculosa* and *F. palustris* are important both from scientific and practical aspects in terms of wood protection. In this study, the differences between *F. radiculosa*, which dramatically lowered the copper concentration during growth and *F. palustris*, which grew vigorously in regions of high copper, suggests that the two species may rely on very different biological processes for copper tolerance. If this were the case, co-biocides developed specifically to block the glyoxylate, tricarboxylic acid, ATP cycle used in copper removal in *Fibroporia* may not necessarily work for *Fomitopsis* (Tang *et al*. 2016) and thus may only work on some copper-tolerant species of fungi (Tang *et al*. 2016). It is conceivable that, depending upon the species, any one or combination of these mechanisms could be contributing to copper tolerance and the differences observed in the XFM elemental maps.

5. Conclusions

These results show how large field-of-view synchrotron-based XFM can be used to better understand mechanisms of copper tolerance in brown rot fungi. The XFM maps showed how different fungi interacted with a copper front in the wood. *F. radiculosa* was able to colonize the copper-rich region of wood and greatly reduced the copper concentration in that area. Conversely, *G. trabeum* avoided the copper region. While *F. palustris* and *P. placenta* were able to colonize the copper-rich wood, they had a much smaller effect on the copper concentration. These interspecies differences in fungal–copper interactions had not been previously observed and suggest possible differences in the mechanisms of copper tolerance across copper-tolerant brown rot fungi. Future work utilizing high-resolution XFM could help determine the role of oxalate in copper tolerance by showing whether copper-oxalate crystals are formed and whether there are differences in these crystals between the fungi examined. This set of experiments serves as a theoretical exposure of Cu preservatives and a more realistic exposure would be actual preserving chemicals but the presence of added co-biocides can complicate results. Future experiments that take into consideration actual treating solutions are in the planning stages.

Disclosure statement

No potential conflict of interest was reported by the authors.

Funding

The use of Advanced Photon Source facilities was supported by the US Department of Energy and Climate Change, Basic Energy Sciences, Office of Science [contract number W-31-109-Eng-38].

References

Anon. (2017) 4 – Protection of the bio-based material A2 – Jones, Dennis. In C. Brischke (ed.) *Performance of Bio-Based Building Materials* (Cambridge, MA: Woodhead Publishing), pp. 187–247.

Argüello, J. M., Eren, E. and González-Guerrero, M. (2007) The structure and function of heavy metal transport P1B-ATPases. *Biometals*, 20(3–4), 233–248.

Bernicchia, A., Gorjón, S. P., Vampola, P., Ryvarden, L. and Prodi, A. (2012) A phylogenetic analysis of Antrodia sl based on nrDNA ITS sequences, with emphasis on rhizomorphic European species. *Mycological Progress*, 11(1), 93–100.

Burkholder, M. (2004) CCA, NFBA, and the post-frame building industry. *Frame Building News*, 16(5), 6–12.

Clausen, C. A., Green, F., Woodward, B. M., Evans, J. W. and DeGroot, R. C. (2000) Correlation between oxalic acid production and copper tolerance in *Wolfiporia cocos*. *International Biodeterioration & Biodegradation*, 46(1), 69–76.

Clausen, C. A. and Green, F., III (2003) Oxalic acid overproduction by copper-tolerant brown-rot basidiomycetes on southern yellow pine treated with copper-based preservatives. *International Biodeterioration & Biodegradation*, 51(2), 139–144.

Duddridge, J., Malibari, A. and Read, D. (1980) Structure and function of mycorrhizal rhizomorphs with special reference to their role in water transport. *Nature*, 287, 834–836.

Green, F., III and Clausen, C. A. (2003) Copper tolerance of brown-rot fungi: Time course of oxalic acid production. *International Biodeterioration & Biodegradation*, 51(2), 145–149.

Guillén, Y. and Machuca, Á. (2008) The effect of copper on the growth of wood-rotting fungi and a blue-stain fungus. *World Journal of Microbiology and Biotechnology*, 24(1), 31–37.

Hastrup, A. C. S., Green III, F., Clausen C. A. and Jensen, B. (2005) Tolerance of *Serpula lacrymans* to copper-based wood preservatives. *International Biodeterioration & Biodegradation*, 56(3), 173–177.

Humar, M., Petrič, M., Pohleven, F., Šentjurc, M. and Kalan, P. (2002) Changes of EPR spectra of wood impregnated with copper-based preservatives during exposure to several wood-rotting fungi. *Holzforschung*, 56(3), 229–238. doi:10.1515/HF.2002.038

Humar, M., Šentjurc, M., Amartey, S. A. and Pohleven, F. (2005) Influence of acidification of CCB (Cu/Cr/B) impregnated wood on fungal copper tolerance. *Chemosphere*, 58(6), 743–749. doi:10.1016/j.chemosphere.2004.09.031

Jellison, J., Connolly, J., Goodell, B., Doyle, B., Illman, B., Fekete, F., and Ostrofsky, A. (1997) The role of cations in the biodegradation of wood by the brown rot fungi. *International Biodeterioration & Biodegradation*, 39(2), 165–179.

Jones D. and C. Brishke (2017) Introduction to the performance of bio-based building materials. In Jones, D., Brischke, C. (eds) *Performance of Bio-based Building Materials*. Cambridge, MA: Woodhead Publishing, 1–15.

Kirker, G., Zelinka, S., Gleber, S.-C., Vine, D., Finney, L., Chen, S., Hong, Y. P., Uyarte, O., Vogt, S., Jellison, J., Goodell, B. and Jakes, J. E. (2017) Synchrotron-based X-ray fluorescence microscopy enables multiscale spatial visualization of ions involved in fungal lignocellulose deconstruction. *Scientific Reports*, 7.

Lebow, S. (2004) *Alternatives to chromated copper arsenate for residential construction*. Res. Pap. FPL-RP-618. Madison, WI: USDA Forest Service, Forest Products Laboratory.

Lebow, S. (2010) Wood preservation. In *Wood Handbook – Wood as an Engineering Material*. Madison, WI: U.S. Department of Agriculture, Forest Service, Forest Products Laboratory, 508 pp.

Lebow, S., Woodward, B., Kirker, G. and Lebow, P. (2013) Long-term durability of pressure-treated wood in a severe test site. *Advances in Civil Engineering Materials*, 2(1), 178–188.

Murphy, R. and Levy, J. (1983) Production of copper oxalate by some copper tolerant fungi. *Transactions of the British Mycological Society*, 81(1), 165–168.

Ohno, K., Clausen, C. A., Green, F., and Stanosz, G. (2016) The copper transporting ATPase pump and its potential role in copper-tolerance. *The 47th annual meeting of the International Group on Wood Protection*. Lisbon, Portugal: IRG Secretariat.

Ostrofsky, A., Jellison, J., Smith, K. T. and Shortle, W. C. (1997) Changes in cation concentrations in red spruce wood decayed by brown rot and white rot fungi. *Canadian Journal of Forest Research*, 27(4), 567–571.

Schilling, J. S. and Inda, J. (2011) Assessing the relative bioavailability of copper to fungi degrading treated wood. *International Biodeterioration & Biodegradation*, 65(1), 18–22.

Schilling, J. S. and Jellison, J. (2007) Extraction and translocation of calcium from gypsum during wood biodegradation by oxalate-producing fungi. *International Biodeterioration & Biodegradation*, 60(1), 8–15.

Tang, J. D., Parker, L. A., Perkins, A. D., Sonstegard, T. S., Schroeder, S. G., Nicholas, D. D. and Diehl, S. V. (2013) Gene expression analysis of copper tolerance and wood decay in the brown rot fungus *Fibroporia radiculosa*. *Applied and Environmental Microbiology*, 79(5), 1523–1533.

Tang, J. D., Ciaramitaro, T., Nicholas, D. D., Tomaso-Peterson, M. and Diehl, S. V. (2016) Defeating copper tolerance: An example of how "omics" research can accelerate discovery of new wood protection compounds. *Proceedings of the 112th annual meeting of the American Wood Protection Association*. San Juan, PR: American Wood Protection Association.

Vogt, S. (2003) MAPS: A set of software tools for analysis and visualization of 3D X-ray fluorescence data sets. *Journal de physique. IV*, 104, 635–638.

Zelinka, S. L. (2014) Chapter 23. Corrosion of metals in wood products. In M. Aliofkhazraei (ed.) *Developments in Corrosion Protection* (Rijeka: InTech), pp. 568–592.

Zelinka, S. L., Gleber, S. C., Vogt, S., López, G. M. R. and Jakes, J. E. (2015) Threshold for ion movements in wood cell walls below fiber saturation observed by X-ray fluorescence microscopy (XFM). *Holzforschung*, 69 (4), 441–448.

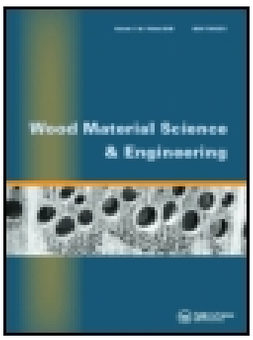

Wood Material Science & Engineering

ISSN: 1748-0272 (Print) 1748-0280 (Online) Journal homepage: http://www.tandfonline.com/loi/swoo20

Fungal–copper interactions in wood examined with large field of view synchrotron-based X-ray fluorescence microscopy

Samuel L. Zelinka, Joseph E. Jakes, Juliet Tang, Katie Ohno, Amy Bishell, Lydia Finney, Evan R. Maxey, Stefan Vogt & Grant T. Kirker

To cite this article: Samuel L. Zelinka, Joseph E. Jakes, Juliet Tang, Katie Ohno, Amy Bishell, Lydia Finney, Evan R. Maxey, Stefan Vogt & Grant T. Kirker (2018): Fungal–copper interactions in wood examined with large field of view synchrotron-based X-ray fluorescence microscopy, Wood Material Science & Engineering, DOI: 10.1080/17480272.2018.1458049

To link to this article: https://doi.org/10.1080/17480272.2018.1458049